

A Systematic Framework for Natural Perturbations from Videos

Vaishaal Shankar*
UC Berkeley

Achal Dave*
CMU

Rebecca Roelofs
UC Berkeley

Deva Ramanan
CMU

Benjamin Recht
UC Berkeley

Ludwig Schmidt
UC Berkeley

Abstract

We introduce a systematic framework for quantifying the robustness of classifiers to image perturbations that naturally occur in videos. As part of this framework, we construct ImageNet-Vid-Robust, a dataset of 22,178 images grouped into 1,109 sets of perceptually similar images. The dataset was derived from the ImageNet Video Object Detection dataset and annotated by human experts. We evaluate a diverse array of classifiers pre-trained on ImageNet and show a median classification accuracy drop of 16%. Additionally, we evaluate three detection models and show that natural perturbations induce both classification as well as localization errors, leading to a median drop in detection mAP of 14 points. Our analysis demonstrates that perturbations occurring naturally in videos pose a substantial challenge to deploying convolutional neural networks in environments that require both reliable and low-latency predictions.

1 Introduction

Despite their strong performance on various computer vision benchmarks, convolutional neural networks (CNNs) still exhibit many troubling failure modes. At one extreme, ℓ_p -adversarial examples cause large drops in accuracy for state of the art models with visually imperceptible changes to the input image [4, 12]. But since carefully crafted ℓ_p -perturbations are unlikely to occur naturally in the real world, they usually do not pose a problem outside a fully adversarial context.

To study more realistic failure modes, researchers have investigated benign image perturbations such as rotations & translations, colorspace changes, and various image corruptions [8, 15, 16]. However, it is still unclear whether these perturbations reflect the robustness challenges commonly arising in real data since the perturbations still rely on synthetic image modifications.

Recent work has therefore turned to videos as a source of *naturally occurring* perturbations of images [2, 13]. In contrast to other failure modes, the perturbed images are taken from existing image data without further modifications that make the task more difficult. As a result, robustness to such perturbations directly corresponds to performance improvements on real data.

*Equal contribution

However, it is currently unclear to what extent such video perturbations pose a significant robustness challenge. Azulay and Weiss [2] only provide anecdotal evidence from a small number of videos. Gu et al. [13] work with a larger video dataset to obtain accuracy estimates, but they observe a drop in accuracy of around 3% on video-perturbed images. This small drop suggests that perturbations occurring in videos may not substantially reduce the accuracy of current CNNs.

We address this question by conducting a thorough evaluation of robustness to natural perturbations arising in videos. As a cornerstone of our investigation, we introduce ImageNet-Vid-Robust, a carefully curated subset of ImageNet-Vid [29]. All images in ImageNet-Vid-Robust were screened by a set of expert labelers to ensure high annotation quality and minimize selection biases that arise when filtering a dataset with CNNs. Overall, ImageNet-Vid-Robust contains 22,178 images grouped into 1,109 sets of temporally adjacent and visually similar images. Similar to ImageNet-Vid, ImageNet-Vid-Robust has 30 classes.

We then utilize ImageNet-Vid-Robust to measure the accuracy of current CNNs to small, naturally occurring perturbations. Our testbed contains over 50 different model types, varying both architecture and training methodology (adversarial training, data augmentation, etc.). To better understand the drop in accuracy due to natural perturbations, we introduce a more stringent robustness metric. On this metric, we find that natural perturbations from ImageNet-Vid-Robust induce a median 16% accuracy drop for classification tasks and a median 14 point drop in mAP for detection tasks. Even for the best-performing classification model, we observe an accuracy drop of 14%.

Our results show that robustness to natural perturbations in videos is indeed a significant challenge for current CNNs. As these models are increasingly deployed in safety-critical environments that require both high accuracy and low latency (e.g., autonomous vehicles), ensuring reliable predictions on *every frame* of a video is an important direction for future work.

2 The ImageNet-Vid-Robust dataset

The ImageNet-Vid-Robust dataset is sourced from videos contained in the ImageNet-Vid dataset [29]. We first provide background on ImageNet-Vid and then describe how we used it to construct ImageNet-Vid-Robust.

2.1 ImageNet-Vid

The 2015 ImageNet-Vid dataset is widely used for training video object detectors [14] as well as trackers [3]. We chose to work with the 2017 ImageNet-Vid dataset because it is a superset of the 2015 dataset. In total, the 2017 ImageNet-Vid dataset consists of 1,181,113 training frames from 4,000 videos and 512,360 validation frames from 1,314 videos. The videos have frame rates ranging from 9 to 59 frames per second (fps), with a median fps of 29. The videos range from 0.44 to 96 seconds in duration with a median duration of 12 seconds. Each frame is annotated with labels indicating the presence or absence of 30 object classes and corresponding bounding boxes for any label present in the frame.

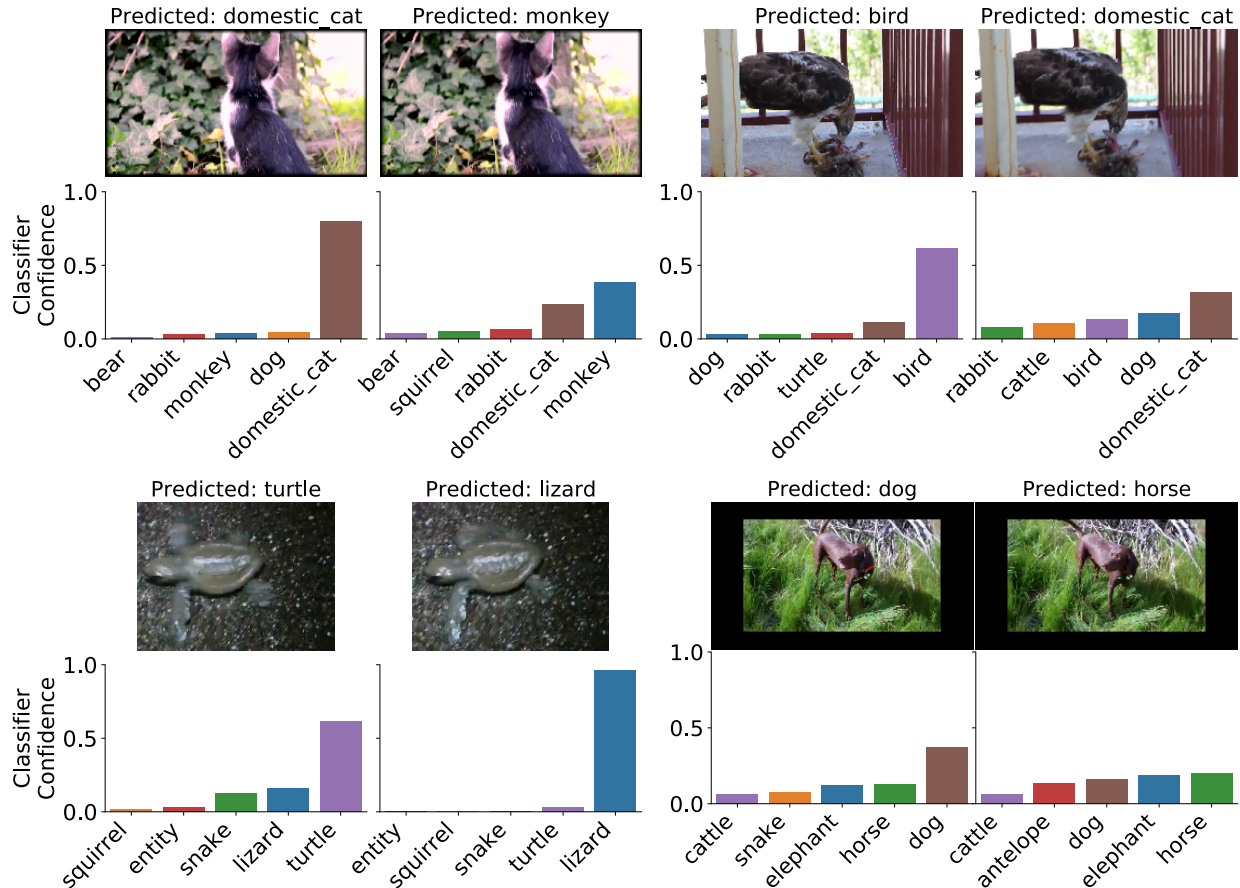


Figure 1: Three examples of natural perturbations from nearby video frames and resulting classifier confidences from a ResNet-152 model fine-tuned on ImageNet-Vid. While the images appear almost identical to the human eye, the classifier confidence changes substantially.

An advantage of using the ImageNet-Vid dataset as the source of our dataset is that all 30 object classes in the ImageNet-Vid dataset are contained within the WordNet hierarchy [24]. These 30 classes are ancestors of 288 of the 1,000 ILSVRC-2012 classes (ImageNet Large Scale Visual Recognition Competition [29]). Using the WordNet hierarchy, we construct a canonical mapping from ILSVRC-2012 classes to ImageNet-Vid classes, which allows us to evaluate several off-the-shelf ILSVRC-2012 models on ImageNet-Vid and ImageNet-Vid-Robust.

2.2 Constructing ImageNet-Vid-Robust

Next, we describe how we extracted neighboring sets of naturally perturbed frames from ImageNet-Vid to create ImageNet-Vid-Robust. A straightforward approach is to select a set of anchor frames and use temporally adjacent frames in the video with the assumption that such frames contain only small perturbations from the anchor frame. However, as Figure 2 illustrates, this assumption is frequently violated, especially in the presence of fast camera or object motion.

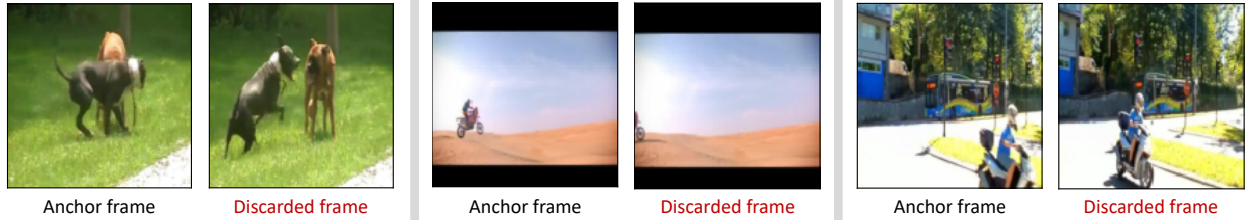


Figure 2: Temporally adjacent frames may not be visually similar. We show three randomly sampled frame pairs where the nearby frame was marked as “dissimilar” to the anchor frame during human review and then discarded from our dataset.

Instead, we collect a preliminary dataset of natural perturbations and then manually review each of the frame sets. For each video, we randomly sample an anchor frame and take $k = 10$ frames before and after the anchor frame as candidate perturbation images. This results in a dataset containing one anchor frame each from 1,314 videos, with approximately 20 candidate perturbation per anchor frame.¹

Next, we curate the dataset with the help of four expert human annotators. The goal of the curation step is to ensure that each anchor frame and its nearby frames are correctly labeled with the same ground truth class, and that the anchor frame and the nearby frames are visually similar. So for each pair of anchor and candidate perturbation frames, a human annotator labels (1) whether the pair is correctly labeled in the dataset, (2) whether the pair is similar.

Asking human annotators to label whether a pair of frames is similar can be highly subjective. We took several steps to mitigate this issue and ensure high annotation quality. First, we trained reviewers to mark frames as dissimilar if the scene undergoes any of the following transformations: significant motion, significant background change, or significant blur change. We asked reviewers to mark each dissimilar frame with one of these transformations, or “other”. Second, we present only a single pair of frames at a time to reviewers because presenting videos or groups of frames could cause them to miss large changes due to the phenomenon of change blindness [25].

Finally, to increase consistency in annotation, human annotators proceeded in two rounds of review. In the first round, all annotators were given identical labeling instructions and then individually reviewed 6,500 images pairs. We instructed annotators to err on the side of marking a pair of images as dissimilar if a distinctive feature of the object is only visible in one of the two frames (such as the face of a dog). If an annotator was unsure about a pair, she could mark the pair as “don’t know”. For the second round of review, all annotators jointly reviewed *all* frames marked as dissimilar, “don’t know”, or incorrect. A frame was only considered similar to its anchor if a strict majority of the annotators marked the pair as such.

After the reviewing was complete, we discarded all anchor frames and candidate perturbations that annotators marked as dissimilar or incorrectly labeled. Our final dataset contains 1,145 anchor frames with a minimum of 1, maximum of 20, and median of 20 similar frames.

¹Anchor frames near the start or end of the video may have less than 20 candidate frames.

3 The pm-k evaluation metric

Given the ImageNet-Vid-Robust dataset introduced above, we propose a metric to measure a model’s robustness to natural perturbations. In particular, let $A = \{a_1, \dots, a_n\}$ be the set of valid anchor frames in our dataset. Let $Y = \{y_1, \dots, y_n\}$ be the set of labels for A . We let $\mathcal{N}_k(a_i)$ be the set of frames marked as similar to anchor frame a_i . In our setting, \mathcal{N}_k is a subset of the $2k$ temporally adjacent frames (plus/minus k frames from the anchor).

Classification. Classification accuracy is defined as

$$\text{acc}_{\text{orig}} = 1 - \frac{1}{N} \sum_{i=0}^N \mathcal{L}_{0/1}(f(a_i), y_i), \quad (1)$$

where $\mathcal{L}_{0/1}$ is the standard 0-1 loss function. We define the pm-k analog of accuracy as

$$\text{acc}_{\text{pmk}} = 1 - \frac{1}{N} \sum_{i=0}^N \max_{b \in \mathcal{N}_k(a_i)} \mathcal{L}_{0/1}(f(b), y_i), \quad (2)$$

which simply corresponds to picking the worst frame from each set $\mathcal{N}_k(a_i)$ before computing accuracy.

Detection. The standard metric for detection is mean average precision (mAP) of the predictions at a fixed intersection-over-union (IoU) threshold [21]. We briefly introduce the metric here and refer the reader to [20] for further details.

The standard detection metric proceeds by first determining whether each predicted bounding box in an image is a true or false positive, based on the intersection over union (IoU) of the predicted and ground truth bounding boxes. The metric then computes the per-category average precision (AP, averaged over recall thresholds) of the predictions across all images. The final metric is reported as the mean of these per-category APs (mAP), which we denote $\text{mAP}(\{f(a_i), y_i\}_{i=0}^N)$.

We define the pm-k analog of mAP by replacing each anchor frame in the dataset with a nearby frame that minimizes the per-image average precision. Since the category-specific average precision is undefined for categories not present in an image, we minimize the average precision across categories present in each frame rather than the mAP. We then define the pm-k mAP as follows, using y_b to denote the label for frame b :

$$\text{mAP}_{\text{pmk}}(\{f(a_i), y_i\}_{i=0}^N) = \text{mAP} \left(\left\{ \argmin_{b \in \mathcal{N}(a_i)} AP(f(b), y_b) \right\}_{i=0}^N \right). \quad (3)$$

4 Main results

We evaluate a testbed of 50 classification and three detection models on ImageNet-Vid-Robust. We first discuss the various types of classification models evaluated with the pm-k classification

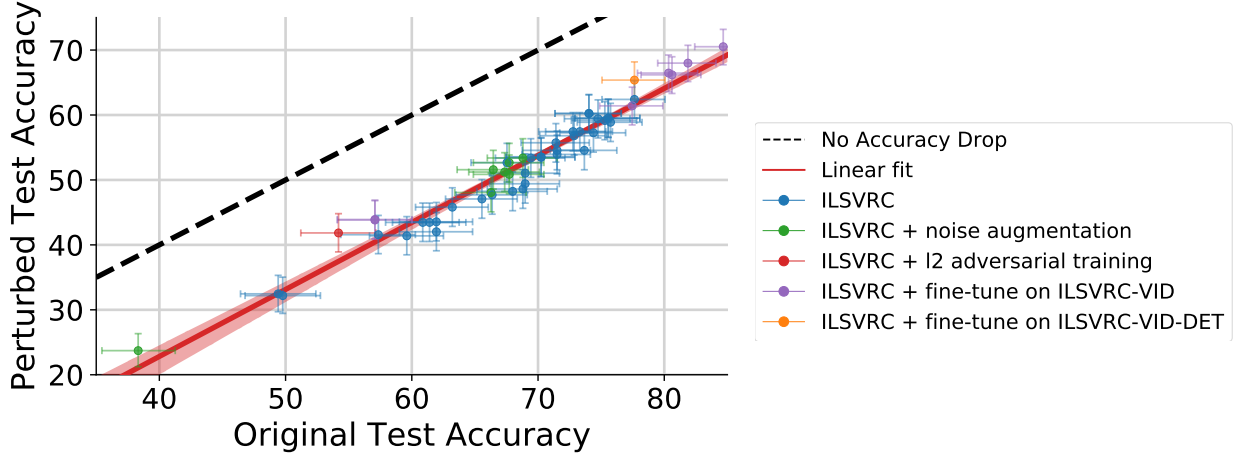


Figure 3: Model accuracy on original vs. perturbed images. Each data point corresponds to one model in our testbed (shown with 95% Clopper-Pearson confidence intervals). Each perturbed frame was taken from a ten frame neighborhood of the original frame (approximately 0.3 seconds). All frames were reviewed by humans to confirm visual similarity to the original frames.

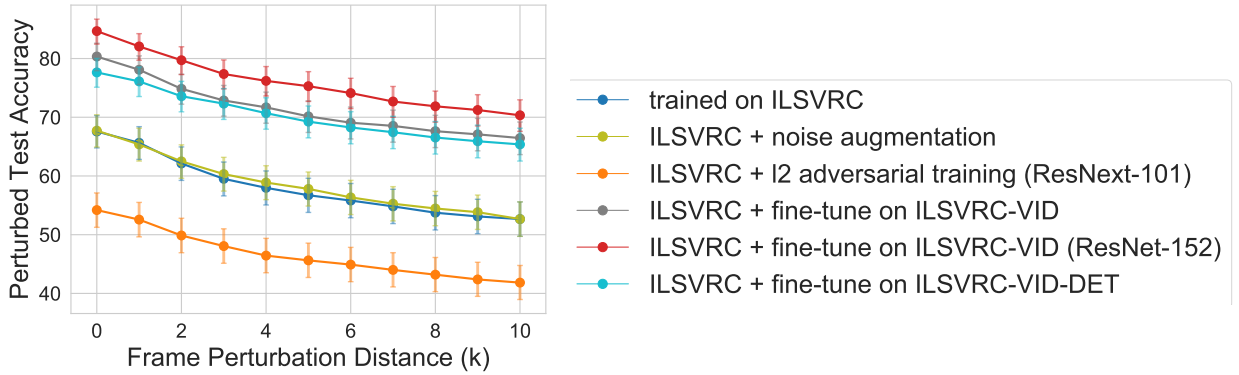


Figure 4: Model classification accuracy on perturbed frames as a function of perturbation distance (shown with 95% Clopper-Pearson confidence intervals). Model accuracies from five different model types and the best performing model are shown. The model architecture is ResNet-50 unless otherwise mentioned.

metric. Second, we use the bounding box annotations inherited from ImageNet-Vid to study the performance of detection models evaluated on ImageNet-Vid-Robust using the pm-k detection metric. We then analyze the errors made on the detection adversarial examples to isolate the effects of *localization* errors vs. *classification* errors.

4.1 Classification

The classification robustness metric is acc_{pmk} defined in Equation (2). In Figure 3, we plot acc_{orig} versus acc_{pmk} for all classification models in our test bed and find that the relationship between

Table 1: Accuracies of five different model types and the best performing model. The model architecture is ResNet-50 unless noted otherwise. See Section 4.1 for details.

Model Type	Accuracy Original	Accuracy Perturbed	Δ
Trained on ILSVRC	67.5 [64.7, 70.2]	52.7 [49.7, 55.6]	14.9
ILSVRC + noise augmentation	67.7 [64.9, 70.4]	52.7 [49.7, 55.6]	15.1
ILSVRC + ℓ_∞ robustness (ResNext-101)	54.2 [51.3, 57.1]	41.8 [39.0, 44.8]	12.4
ILSVRC + fine-tune on ImageNet-Vid	81.9 [79.5, 84.1]	68.0 [65.2, 70.7]	13.9
ILSVRC + fine-tune on ImageNet-Vid (ResNet-152)	84.7 [82.5, 86.7]	70.5 [67.8, 73.1]	14.2
ILSVRC + fine-tune on ImageNet-Vid-Det	77.6 [75.1, 80.0]	65.4 [62.5, 68.1]	12.3

acc_{orig} and acc_{pmk} is approximately linear.

In Figure 4, we plot the relationship between acc_{pmk} and perturbation distance (i.e., the k in the pm-k metric). The entire x-axis in Figure 4 corresponds to a temporal distance of at most 0.3 seconds between the original and perturbed frames.

Among the 22,668 frames in ImageNet-Vid-Robust, 1,578 frames have multiple correct classification labels due to the presence of multiple objects in the frame. We count a prediction as correct if the model predicts *any* of the correct classes for a frame.

We considered five models types with increasing levels of supervision. We present the accuracy numbers for representative models from each model type in Table 1 and defer the full classification results table to Appendix A.

Trained on ILSVRC. As mentioned in Section 2.1, the WordNet hierarchy enables us to utilize models originally trained for the 1,000 class ILSVRC-2012 dataset on our new dataset ImageNet-Vid-Robust. We evaluate a wide array of ILSVRC-2012 models (available from [5]) against our natural perturbations. Since ImageNet-Vid-Robust (and already ImageNet-Vid) has a substantial distribution shift from the original ILSVRC-2012 validation, we expect the *benign* accuracy acc_{orig} to be lower than the comparable accuracy on the ILSVRC-2012 validation set. However, the main quantity of interest here is the the *difference* between the original and perturbed accuracies $\text{acc}_{\text{orig}} - \text{acc}_{\text{pmk}}$. A small drop in accuracy would indicate that the model is robust to small changes that occur naturally in videos. We instead find a significant 14.9% drop in accuracy, indicating brittleness to such changes.

Trained on ILSVRC with noise augmentation. One hypothesis for the accuracy drop from original to perturbed accuracy is that subtle artifacts and corruptions introduced by video compression schemes could degrade performance when evaluating on these corrupted frames. The worst-case nature of the pm-k metric could then be focusing on these corrupted frames. One model for these corruptions are the perturbations introduced in [15]. To test this hypothesis, we evaluate models augmented with a subset of the perturbations (exactly one of: Gaussian noise, Gaussian blur, shot noise, contrast change, impulse noise, or JPEG compression) found in [15]. We found that these

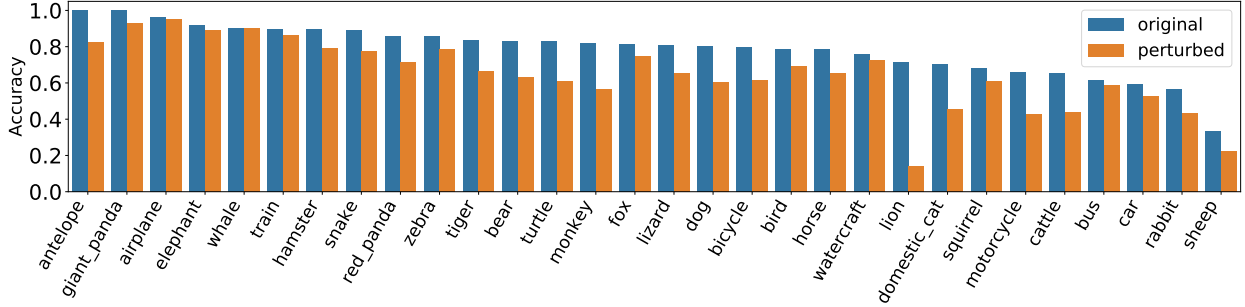


Figure 5: Per-class accuracy statistics for our best performing classification model (fine-tuned ResNet152) on ImageNet-Vid-Robust,

augmentation schemes did not improve robustness against our perturbations substantially, and still result in an accuracy drop of 15.1%.

Trained on ILSVRC for ℓ_2/ℓ_∞ robustness. We evaluate the model that currently performs best against ℓ_2/ℓ_∞ attacks on ImageNet [33]. We find that this model has a slightly smaller accuracy drop than the two aforementioned model types (ILSVRC and ILSVRC + noise augmentation), but the difference is well within the error bars induced by the size of the test set. We also note that this robust model achieves significantly lower original and perturbed accuracy than either of the two model types above.

Trained on ILSVRC and fine-tuned on ImageNet-Vid. To adapt to the 30 class problem and the different domain of videos, we fine-tune several network architectures on the ImageNet-Vid training set. We trained with the largest object in the scene as the label during training because we found this approach performed better than training using a multi-label loss function. We provide hyperparameters for all models in Appendix D. The resulting models improve in absolute accuracy over their ILSVRC pre-trained counterparts (e.g., 12% for a ResNet-50). However, this improvement in absolute accuracy does not significantly decrease the accuracy drop induced by natural perturbations.

Trained on ILSVRC and fine-tuned on ImageNet-Vid-Det. We analyze whether additional supervision in the form of bounding box annotations improves robustness. To this end, we train the Faster R-CNN *detection* model [28] with a ResNet-50 backbone on ImageNet-Vid. Following standard practice, the detection backbone is pre-trained on ILSVRC-2012. To evaluate this detector for classification, we assign the class with the most confident bounding box as label to the image. We find that this transformation reduces accuracy compared to the model trained for classification (76.3% vs. 79.5%). While there is a slight reduction in the accuracy drop caused by natural perturbations, the reduction is well within the error bars for this test set.

Per-class accuracies. We study the effect of our perturbations on the 30 classes in our dataset to determine whether the performance drop was concentrated in a few “hard” classes. Figure 5 shows

Table 2: Detection and localization mAP for two Faster R-CNN backbones. Both detection and localization suffer from significant drops in mAP due to the perturbations. (*Model trained on ILSVRC Det and VID 2015 datasets, and evaluated on a subset of ILSVRC-VID 2017 videos corresponding to the 2015 version of the dataset.)

Model	mAP Original	mAP Perturbed	mAP Δ
FRCNN, ResNet 50	62.8	48.8	14.0
FRCNN, ResNet 101	63.1	50.6	12.5
R-FCN, ResNet 101 [32]*	79.4*	63.7*	15.7*
FRCNN, ResNet 50 - Localization	76.6	64.2	12.4
FRCNN, ResNet 101 - Localization	77.8	66.3	11.5
R-FCN, ResNet 101 - Localization [32]*	80.9*	70.3*	10.6*

the original and perturbed accuracies across classes for our best performing model (a fine-tuned ResNet-152). This model saw a total drop of 13.7% between original and perturbed images and a median drop of 12.1% in per-class accuracy. Although there are a few particularly difficult classes for perturbed accuracy (e.g., lion or monkey), the accuracy drop is spread across most classes.

4.2 Detection

To investigate the effect of natural perturbations on further tasks, we now study their impact on object detection. Specifically, we report results for two related tasks: object localization and detection. Object detection is the standard computer vision task of correctly classifying an object and finding the coordinates of a tight bounding box containing the object. “Object localization”, meanwhile, refers to only the subtask of finding the bounding box, *without* attempting to correctly classify the object. This is an important problem from a practical perspective (for example, the size and location of an obstacle may be more important for navigation than the category), as well as from an analytical perspective, as it allows analyzing mistakes orthogonal to classification errors. For instance, it may be the case that natural perturbations cause misclassification errors frequently (e.g., it may be natural to mistake a cat for a fox), but cause localization errors only rarely.

We present our results using the popular Faster R-CNN [28] and R-FCN [7, 32] architectures for object detection and localization in Table 2. For the R-FCN architecture, we use the model from [32].² We first note the significant drop in mAP of 12 – 15 points for object detection due to perturbed frames for both the Faster R-CNN and R-FCN architectures. Next, we show that localization is indeed easier than detection, as the mAP is higher for localization than for detection (e.g., 76.6 vs 62.8 for Faster R-CNN with a ResNet-50 backbone). Perhaps surprisingly, however, switching to the localization task does *not* improve the drop between original and perturbed frames, indicating that natural perturbations induce both classification and localization errors. We show examples of detection failures in Figure 6.

²This model was originally trained on the 2015 subset of ImageNet-Vid. We evaluated this model on the 2015 validation set because the method requires access to pre-computed bounding box proposals which are available only for the 2015 subset of ImageNet-Vid.



Figure 6: Naturally perturbed examples for detection. Red boxes indicate false positives; green boxes indicate true positives; white boxes are ground truth. Classification errors are one of the most common failures, such as the fox on the left, which is classified correctly in the anchor frame, and misclassified as a sheep in the nearby frame. However, detection models also have *localization* errors, where the object of interest is not correctly localized in addition to being misclassified, such as the airplane (middle) and the motorcycle (right). All visualizations show predictions with confidence greater than 0.5.

5 Related work

Adversarial examples. While various forms of adversarial examples have been studied, the majority of research focuses on ℓ_p robustness [4, 12]. In the ℓ_p model, the attacker adds a perturbation vector δ such that $\|\delta\|_p < \epsilon$, where ϵ is generally chosen such that the perturbation is (almost) imperceptible to a human. Adversarial attacks in the ℓ_p model are powerful and difficult to defend against. For instance, the state of the art defenses still achieve mediocre classification accuracies on adversarial inputs (below 65% on CIFAR-10 [1, 6, 22, 31, 34]).

Motivated by the artificial nature of ℓ_p attacks, recent work has proposed more realistic image modifications such as small rotations & translations [2, 8, 9, 18], hue and color changes [16], and common image corruptions such as Gaussian blur and JPEG compression [11, 15]. Researchers have also successfully used generative adversarial networks (GANs) to synthesize adversarial examples [35]. Even though the above examples are more realistic than the ℓ_p model, they still synthetically modify the input images to generate perturbed versions. In contrast, our work performs no synthetic modification and instead uses images that naturally occur in videos.

Utilizing videos to study robustness. Azulay and Weiss [2] highlight videos as a failure case of CNNs and provide qualitative examples where models misclassify adjacent video frames (similar to Figure 1). In work concurrent to ours, Gu et al. [13] exploit the temporal structure in videos to

study robustness. However, their experiments suggest a substantially smaller drop in classification accuracy. The primary reason for this is a less stringent metric used in [13]. By contrast, our “pm-k” metric is inspired by the “worst-of-k” metric used in prior work [8], highlighting the brittleness of models to natural perturbations. Further, Gu et al. [13] evaluate on the YoutubeBB dataset [26], which is constructed by filtering YouTube videos with CNNs. This dataset filtering could introduce selection bias towards videos that are easier to classify with CNNs, possibly resulting in overly optimistic robustness evaluations. In contrast, ImageNet-Vid [29], from which we derive ImageNet-Vid-Robust, is constructed through human review of YouTube videos. To the best of our knowledge, there was also no exhaustive human verification of the adversarial frames in [13], while all perturbed images in our dataset were verified by humans to be similar to the corresponding anchor frame.

Distribution shift. Small, benign changes in the test distribution are often referred to as *distribution shift*. Recht et al. [27] explore this phenomenon by constructing new test sets for CIFAR-10 and ImageNet and observe performance drops for a large suite of models on the newly constructed test sets. Similar to our Figure 3, the relationship between original and new test set accuracy is also approximately linear. However, the images in their test set bear little visual similarity to images in the original test set, while all of our failure cases in ImageNet-Vid-Robust are on perceptually similar images. In a similar vein of study, [30] studies distribution shift *across* different computer vision data sets such as Caltech-101, PASCAL 2007, ImageNet and many others.

Computer vision. The sensitivity of models to small perturbations in videos has been a focus of attention in the computer vision community. A common issue when applying image based models to videos is *flickering*, where object detectors spuriously produce false-positives or false-negatives in isolated frames or groups of frames. Jin et. al. [17] explicitly identify such failures and use a technique reminiscent of adversarially robust training to improve image-based models. A similar line of work focuses on improving object detection in videos as objects become occluded or move quickly [10, 19, 32, 36]. The focus in this line of work has generally been on improving object detection when objects transform in a way that makes recognition difficult from a single frame, such as fast motion or occlusion. In this work, we document a broader set of failure cases for image-based classifiers and detectors and show that failures occur when the neighboring frames are imperceptibly different.

6 Discussion

Modern machine learning methods are increasingly put to use in challenging, safety-critical environments. Understanding and measuring the sensitivity of these methods in the real world is crucial for building robust and reliable machine learning systems. Our work presents a systematic framework for quantifying a model’s sensitivity to *natural perturbations*. Using this framework, we show that these perturbations cause significant drops in accuracy across architectures for both classification and detection. Our work on analyzing this failure mode opens multiple avenues for future research:

Building more robust models. Our ImageNet-Vid-Robust dataset provides a standard measure for robustness that can be applied to any classification or detection model. In Table 1, we evaluated several commonly used models and found that all of them suffer from substantial accuracy drops due to natural perturbations. In particular, we found that model improvements with respect to artificial perturbations (such as image corruptions or ℓ_2/ℓ_∞ adversaries) do *not* yield significantly more robustness to natural perturbations. We hope that our standardized dataset and evaluation metric will enable future work to quantify improvements in natural robustness directly.

Further natural perturbations. Videos provide a straightforward method for collecting natural perturbations of images, admitting the study of realistic forms of robustness for machine learning methods. Other methods for generating these natural perturbations are likely to provide additional insights into model robustness. As an example, photo sharing websites contain a large number of near-duplicate images: pairs of images of the same scene captured at different times, viewpoints, or from a different camera [27]. More generally, devising similar, domain-specific strategies to collect, verify, and measure robustness to natural perturbations in domains such as natural language processing or speech recognition is a promising direction for future work.

Acknowledgements

We thank Rohan Taori for providing models trained for robustness to image corruptions, and Pavel Tokmakov for his help with training detection models on ImageNet-Vid. This research was generously supported in part by ONR awards N00014-17-1-2191, N00014-17-1-2401, and N00014-18-1-2833, the DARPA Assured Autonomy (FA8750-18-C-0101) and Lagrange (W911NF-16-1-0552) programs, an Amazon AWS AI Research Award, and a gift from Microsoft Research.

References

- [1] Anish Athalye, Nicholas Carlini, and David Wagner. Obfuscated gradients give a false sense of security: Circumventing defenses to adversarial examples. In *International Conference on Machine Learning (ICML)*, 2018. URL <https://arxiv.org/abs/1802.00420>.
- [2] Aharon Azulay and Yair Weiss. Why do deep convolutional networks generalize so poorly to small image transformations? *arXiv preprint arXiv:1805.12177*, 2018.
- [3] Luca Bertinetto, Jack Valmadre, Joao F Henriques, Andrea Vedaldi, and Philip HS Torr. Fully-convolutional siamese networks for object tracking. In *European conference on computer vision*, pages 850–865. Springer, 2016.
- [4] Battista Biggio and Fabio Roli. Wild patterns: Ten years after the rise of adversarial machine learning. *Pattern Recognition*, 2018. <https://arxiv.org/abs/1712.03141>.
- [5] Remi Cadene. Pretrained models for pytorch. <https://github.com/Cadene/pretrained-models.pytorch>. Accessed: 2019-05-20.

- [6] Yair Carmon, Aditi Raghunathan, Ludwig Schmidt, Percy Liang, and John C Duchi. Unlabeled data improves adversarial robustness. *arXiv preprint arXiv:1905.13736*, 2019.
- [7] Jifeng Dai, Yi Li, Kaiming He, and Jian Sun. R-fcn: Object detection via region-based fully convolutional networks. In *Advances in neural information processing systems*, pages 379–387, 2016.
- [8] Logan Engstrom, Brandon Tran, Dimitris Tsipras, Ludwig Schmidt, and Aleksander Madry. A rotation and a translation suffice: Fooling cnns with simple transformations. *arXiv preprint arXiv:1712.02779*, 2017.
- [9] Alhussein Fawzi and Pascal Frossard. Manitest: Are classifiers really invariant? In *British Machine Vision Conference (BMVC)*, 2015.
- [10] Christoph Feichtenhofer, Axel Pinz, and Andrew Zisserman. Detect to track and track to detect. In *Proceedings of the IEEE International Conference on Computer Vision*, pages 3038–3046, 2017.
- [11] Robert Geirhos, Carlos R. M. Temme, Jonas Rauber, Heiko H. Schütt, Matthias Bethge, and Felix A. Wichmann. Generalisation in humans and deep neural networks. In *Advances in Neural Information Processing Systems (NeurIPS)*. 2018. <http://papers.nips.cc/paper/7982-generalisation-in-humans-and-deep-neural-networks.pdf>.
- [12] Ian J Goodfellow, Jonathon Shlens, and Christian Szegedy. Explaining and harnessing adversarial examples. *arXiv preprint arXiv:1412.6572*, 2014.
- [13] Keren Gu, Brandon Yang, Jiquan Ngiam, Quoc Le, and Jonathan Shlens. Using videos to evaluate image model robustness. *arXiv preprint arXiv:1904.10076*, 2019.
- [14] Wei Han, Pooya Khorrami, Tom Le Paine, Prajit Ramachandran, Mohammad Babaeizadeh, Honghui Shi, Jianan Li, Shuicheng Yan, and Thomas S Huang. Seq-nms for video object detection. *arXiv preprint arXiv:1602.08465*, 2016.
- [15] Dan Hendrycks and Thomas Dietterich. Benchmarking neural network robustness to common corruptions and perturbations. *arXiv preprint arXiv:1903.12261*, 2019.
- [16] Hossein Hosseini and Radha Poovendran. Semantic adversarial examples. In *Proceedings of the IEEE Conference on Computer Vision and Pattern Recognition Workshops*, pages 1614–1619, 2018.
- [17] SouYoung Jin, Aruni RoyChowdhury, Huaizu Jiang, Ashish Singh, Aditya Prasad, Deep Chakraborty, and Erik Learned-Miller. Unsupervised hard example mining from videos for improved object detection. In *ECCV*, 2018.
- [18] Can Kanbak, Seyed-Mohsen Moosavi-Dezfooli, and Pascal Frossard. Geometric robustness of deep networks: analysis and improvement. *arXiv preprint arXiv:1711.09115*, 2017.
- [19] Kai Kang, Hongsheng Li, Tong Xiao, Wanli Ouyang, Junjie Yan, Xihui Liu, and Xiaogang Wang. Object detection in videos with tubelet proposal networks. In *Proceedings of the IEEE Conference on Computer Vision and Pattern Recognition*, pages 727–735, 2017.

- [20] Tsung-Yi Lin, Michael Maire, Serge Belongie, James Hays, Pietro Perona, Deva Ramanan, Piotr Dollár, and C Lawrence Zitnick. MS COCO detection evaluation. <http://cocodataset.org/#detection-eval>. Accessed: 2019-05-16.
- [21] Tsung-Yi Lin, Michael Maire, Serge Belongie, James Hays, Pietro Perona, Deva Ramanan, Piotr Dollár, and C Lawrence Zitnick. Microsoft coco: Common objects in context. In *European conference on computer vision*, pages 740–755. Springer, 2014.
- [22] Aleksander Madry, Aleksandar Makelov, Ludwig Schmidt, Dimitris Tsipras, and Adrian Vladu. Towards deep learning models resistant to adversarial attacks. *ICLR*, 2018.
- [23] Francisco Massa and Ross Girshick. maskrcnn-benchmark: Fast, modular reference implementation of Instance Segmentation and Object Detection algorithms in PyTorch. <https://github.com/facebookresearch/maskrcnn-benchmark>, 2018. Accessed: 2019-05-20.
- [24] George A Miller. Wordnet: a lexical database for english. *Communications of the ACM*, 38(11): 39–41, 1995.
- [25] Harold Pashler. Familiarity and visual change detection. *Perception & psychophysics*, 44(4): 369–378, 1988.
- [26] Esteban Real, Jonathon Shlens, Stefano Mazzocchi, Xin Pan, and Vincent Vanhoucke. Youtube-boundingboxes: A large high-precision human-annotated data set for object detection in video. In *Proceedings of the IEEE Conference on Computer Vision and Pattern Recognition*, pages 5296–5305, 2017.
- [27] Benjamin Recht, Rebecca Roelofs, Ludwig Schmidt, and Vaishaal Shankar. Do imagenet classifiers generalize to imagenet? *arXiv preprint arXiv:1902.10811*, 2019.
- [28] Shaoqing Ren, Kaiming He, Ross Girshick, and Jian Sun. Faster r-cnn: Towards real-time object detection with region proposal networks. In *Advances in neural information processing systems*, pages 91–99, 2015.
- [29] Olga Russakovsky, Jia Deng, Hao Su, Jonathan Krause, Sanjeev Satheesh, Sean Ma, Zhiheng Huang, Andrej Karpathy, Aditya Khosla, Michael Bernstein, Alexander C. Berg, and Li Fei-Fei. ImageNet Large Scale Visual Recognition Challenge. *IJCV*, 115(3):211–252, 2015. doi: 10.1007/s11263-015-0816-y.
- [30] Antonio Torralba, Alexei A Efros, et al. Unbiased look at dataset bias. In *CVPR*, volume 1, page 7. Citeseer, 2011.
- [31] Jonathan Uesato, Jean-Baptiste Alayrac, Po-Sen Huang, Robert Stanforth, Alhussein Fawzi, and Pushmeet Kohli. Are labels required for improving adversarial robustness? *CoRR*, abs/1905.13725, 2019. URL <http://arxiv.org/abs/1905.13725>.
- [32] Fanyi Xiao and Yong Jae Lee. Video object detection with an aligned spatial-temporal memory. In *Proceedings of the European Conference on Computer Vision (ECCV)*, pages 485–501, 2018.
- [33] Cihang Xie, Yuxin Wu, Laurens van der Maaten, Alan Yuille, and Kaiming He. Feature denoising for improving adversarial robustness. *arXiv preprint arXiv:1812.03411*, 2018.

- [34] Hongyang Zhang, Yaodong Yu, Jiantao Jiao, Eric P Xing, Laurent El Ghaoui, and Michael I Jordan. Theoretically principled trade-off between robustness and accuracy. *arXiv preprint arXiv:1901.08573*, 2019.
- [35] Zhengli Zhao, Dheeru Dua, and Sameer Singh. Generating natural adversarial examples. *arXiv preprint arXiv:1710.11342*, 2017.
- [36] Xizhou Zhu, Yujie Wang, Jifeng Dai, Lu Yuan, and Yichen Wei. Flow-guided feature aggregation for video object detection. In *Proceedings of the IEEE International Conference on Computer Vision*, pages 408–417, 2017.

A Full original vs perturbed accuracy for **ImageNet-Vid-Robust**

Model	Accuracy Original	Accuracy Perturbed	Δ
resnet152_finetune	83.7 [81.4, 85.8]	69.7 [66.9, 72.4]	14.0
resnet50_finetune	81.1 [78.7, 83.4]	67.0 [64.1, 69.8]	14.1
resnet50_finetune	79.5 [77.0, 81.8]	65.5 [62.6, 68.3]	14.0
resnet50_finetune	79.5 [77.0, 81.8]	65.2 [62.3, 68.0]	14.2
nasnetalarge	76.7 [74.1, 79.2]	61.3 [58.4, 64.2]	15.4
vgg16_finetune	76.6 [74.0, 79.1]	61.0 [58.1, 63.9]	15.6
resnet50_detection	76.3 [73.7, 78.8]	64.2 [61.3, 67.0]	12.1
inceptionresnetv2	74.8 [72.1, 77.3]	58.0 [55.0, 60.9]	16.8
dpn107	74.6 [71.9, 77.1]	58.7 [55.7, 61.6]	15.9
dpn107	74.6 [71.9, 77.1]	58.7 [55.7, 61.6]	15.9
inceptionv4	74.4 [71.7, 76.9]	58.4 [55.4, 61.3]	16.0
dpn98	73.9 [71.2, 76.5]	58.7 [55.7, 61.6]	15.2
dpn92	73.4 [70.7, 76.0]	56.2 [53.2, 59.1]	17.2
dpn131	73.1 [70.4, 75.7]	59.0 [56.0, 61.9]	14.1
dpn131	73.1 [70.4, 75.7]	59.0 [56.0, 61.9]	14.1
dpn68b	72.6 [69.9, 75.2]	53.6 [50.6, 56.6]	19.0
resnext101	72.4 [69.7, 75.0]	56.8 [53.8, 59.7]	15.6
resnext101	72.1 [69.4, 74.7]	56.0 [53.0, 58.9]	16.1
resnet152	71.9 [69.2, 74.5]	56.3 [53.3, 59.2]	15.5
resnet101	70.7 [67.9, 73.4]	53.3 [50.3, 56.3]	17.5
fbresnet152	70.7 [67.9, 73.4]	53.6 [50.6, 56.6]	17.1
densenet169	70.3 [67.5, 73.0]	54.8 [51.8, 57.8]	15.5
densenet169	69.5 [66.7, 72.2]	52.5 [49.5, 55.5]	17.0
densenet201	69.4 [66.6, 72.1]	52.8 [49.8, 55.8]	16.6
bninception	68.4 [65.6, 71.1]	48.6 [45.6, 51.6]	19.7
densenet121	68.3 [65.5, 71.0]	50.1 [47.1, 53.1]	18.2
dpn68	68.3 [65.5, 71.0]	52.5 [49.5, 55.5]	15.8
nasnetamobile	67.9 [65.1, 70.6]	47.9 [44.9, 50.9]	20.0
resnet50_imagenet_augment_jpeg_compression	67.9 [65.1, 70.6]	52.4 [49.4, 55.4]	15.5
resnet50_imagenet_augment_gaussian_blur	67.1 [64.2, 69.9]	51.7 [48.7, 54.7]	15.4
resnet34	67.0 [64.1, 69.8]	47.5 [44.5, 50.5]	19.5
resnet50_imagenet_augment_impulse_noise	66.9 [64.0, 69.7]	49.9 [46.9, 52.9]	17.0
resnet50	66.8 [63.9, 69.6]	51.9 [48.9, 54.9]	14.9
resnet50_imagenet_augment_gaussian_noise	66.7 [63.8, 69.5]	50.4 [47.4, 53.4]	16.3
resnet50_imagenet_augment_defocus_blur	65.5 [62.6, 68.3]	47.2 [44.2, 50.2]	18.3
resnet50_imagenet_augment_shot_noise	65.4 [62.5, 68.2]	50.6 [47.6, 53.6]	14.8
vgg16_bn	65.4 [62.5, 68.2]	47.0 [44.0, 50.0]	18.4
vgg19_bn	64.7 [61.8, 67.5]	46.4 [43.4, 49.4]	18.3
vgg19_bn	62.5 [59.6, 65.4]	45.3 [42.3, 48.3]	17.2
vgg13_bn	61.1 [58.2, 64.0]	42.8 [39.9, 45.8]	18.3
resnet18	61.0 [58.1, 63.9]	41.2 [38.3, 44.2]	19.8

vgg16	60.6 [57.7, 63.5]	42.9 [40.0, 45.9]	17.7
vgg11	60.1 [57.1, 63.0]	42.8 [39.9, 45.8]	17.3
vgg13	58.7 [55.7, 61.6]	40.8 [37.9, 43.8]	17.9
vgg11	56.9 [53.9, 59.8]	41.0 [38.1, 44.0]	15.8
alexnet_finetune	56.4 [53.4, 59.3]	43.0 [40.1, 46.0]	13.4
feature_denoise	53.7 [50.7, 56.7]	41.4 [38.5, 44.4]	12.3
squeezenet1	49.5 [46.5, 52.5]	32.1 [29.4, 34.9]	17.5
alexnet	49.0 [46.0, 52.0]	32.2 [29.5, 35.0]	16.8
resnet50_imagenet_augment_contrast_change	37.7 [34.8, 40.6]	23.2 [20.7, 25.8]	14.5

Table 3: Classification model perturbed and original accuracies for all models in our test bed.

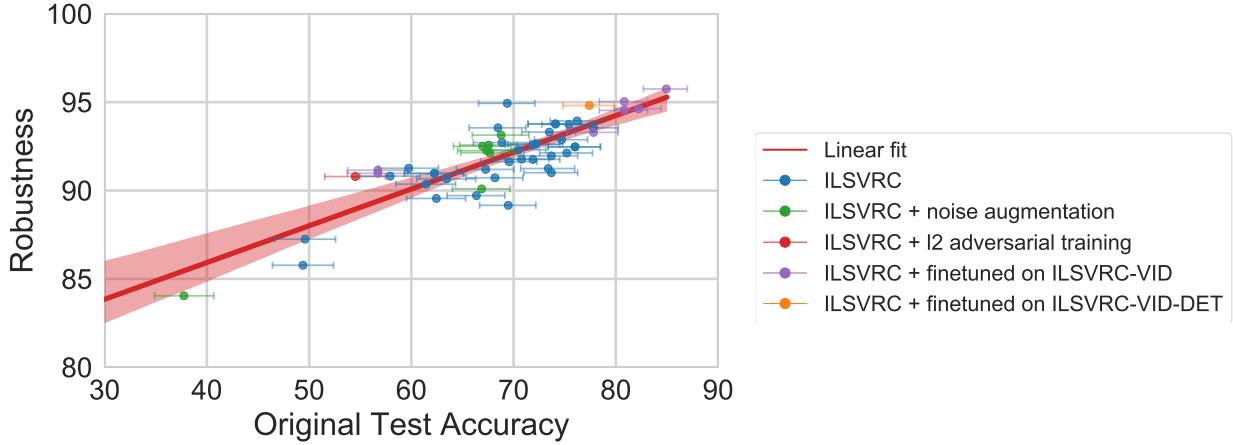


Figure 7: Model accuracy vs. robustness metric introduced in [13]. Each data point corresponds to one model in our testbed (shown with 95% Clopper-Pearson confidence intervals). Each perturbed frame was taken from a ten frame neighborhood of the original frame (approximately 0.3 seconds). All frames were reviewed by humans to confirm visual similarity to the original frames. In this figure we look at a neighborhood of 10 frames around each anchor frame (corresponding to pm-10 in the main text).

B Per-frame conditional robustness metric introduced in [13]

In concurrent work, the authors of [13] considered a different metric of robustness. In this section, we compute this metric on all models in our test bed to compare our findings to [13]. There are two main differences between PM-k and the robustness metric in [13].

1. For two visually similar “neighbor” frames I_0 and I_1 with true label Y and classifier f , [13] studies the conditional probability $P(f(I_1) = y | f(I_0) = y)$
2. While PM-k looks for errors in all neighbor frames in a neighborhood of k frames away from the anchor frame (so this would include frames 1, 2, ..., k frames away), [13] only considers errors from **exactly** k frames away.

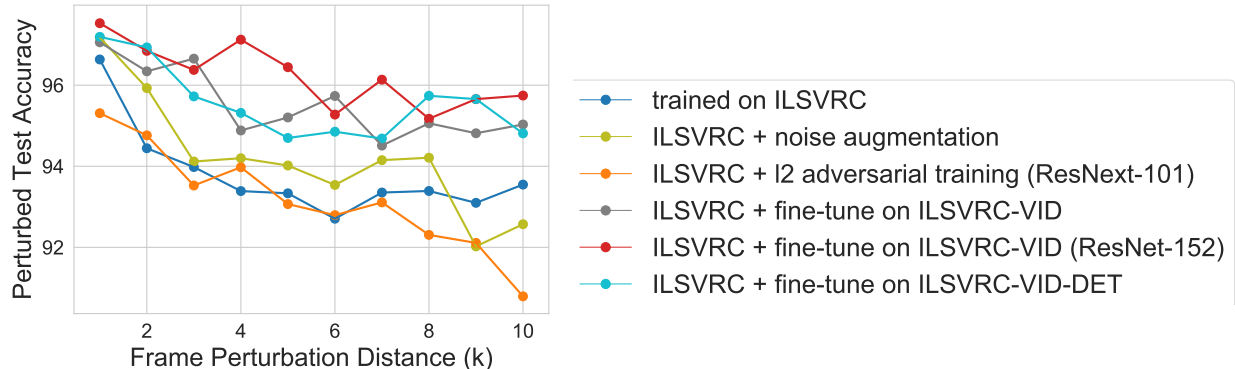


Figure 8: Conditional robustness on perturbed frames as a function of perturbation distance (shown with 95% Clopper-Pearson confidence intervals). Model accuracies from five different model types and the best performing model are shown. The model architecture is ResNet-50 unless otherwise mentioned.

These two distinctions lead to a different measure of robustness across models as shown in Fig. 7 and Fig. 8. Which are the conditional robustness analogues of Figure 3 and Figure 4 in the main text.

C ℓ_∞ distance vs PM-k Accuracy

ℓ_∞ adversarial examples are well studied in the robustness community, yet the connection between ℓ_∞ and other forms of more “natural” robustness is unclear. Here, we plot the cumulative distribution of the ℓ_∞ distance between pairs of nearby frames in our datasets. In Figure 9, we show the CDF of ℓ_∞ distance for all pairs, all reviewed pairs, and mistakes made by 3 indicative models. Note the `fbrobust` model is trained specifically to be robust to ℓ_∞ adversaries.

D Experimental Details & Hyperparameters

All classification experiments were carried out using PyTorch version 1.0.1 on an AWS p3.2xlarge with the NVIDIA V100 GPU. All pretrained models were downloaded from [5] at commit hash 021d97897c9aa76ec759def43d341c4fd45d7ba. Evaluations in Table 3 all use the default settings for evaluation. The hyperparameters for the *fine-tuned* models are presented in Table 4. We searched for learning rates between 10^{-3} and 10^{-5} for all models.

We additionally detail hyperparameters for detection models in Table 5. Detection experiments were conducted with PyTorch version 1.0.1 on a machine with 4 Titan X GPUs, using the Mask R-CNN benchmark repository[23]. We used the default learning rate provided in [23]. For R-FCN, we used the model trained by [32].

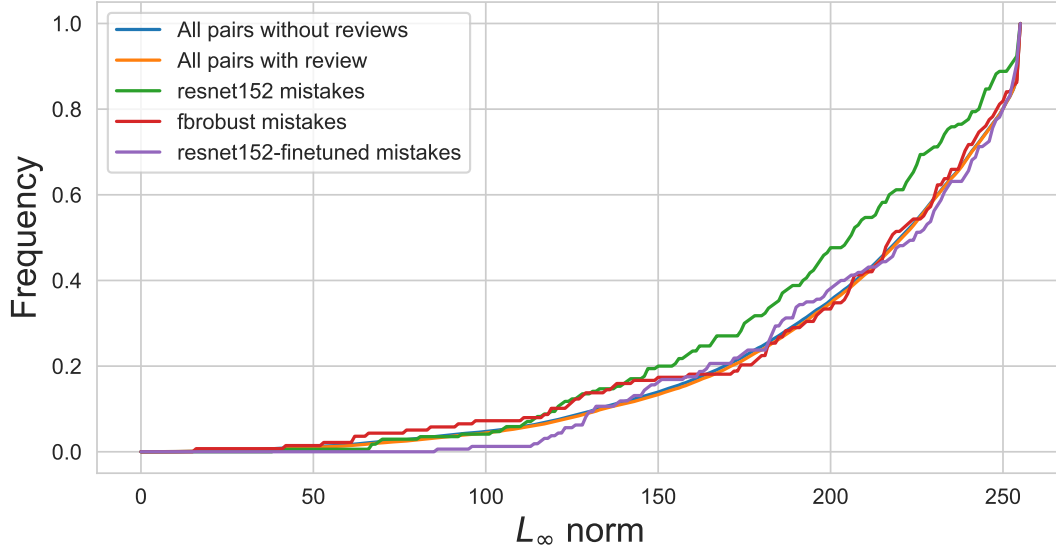


Figure 9: CDF showing the ℓ_∞ distance between pairs of frames from different distributions.

Table 4: Hyperparameters for models finetuned on ImageNet-Vid,

Model	Base Learning Rate	Learning Rate Schedule	Batch Size	Epochs
resnet152	10^{-4}	Reduce LR On Plateau	32	10
resnet50	10^{-4}	Reduce LR On Plateau	32	10
alexnet	10^{-5}	Reduce LR On Plateau	32	10
vgg16	10^{-5}	Reduce LR On Plateau	32	10

Table 5: Hyperparameters for detection models.

Model	Base Learning Rate	Learning Rate Schedule	Batch Size	Iterations
F-RCNN ResNet-50	10^{-2}	Step 20k, 30k	8	40k
F-RCNN ResNet-101	10^{-2}	Step 20k, 30k	8	40k